Journal of Power Sources 202 (2012) 262–268

Contents lists available at SciVerse ScienceDirect

Journal of Power Sources

journal homepage: www.elsevier.com/locate/jpowsour

Synthesis of boron-doped Si particles by ball milling and application in Li-ion batteries

S. Rousselot[a], M. Gauthier[a,b], D. Mazouzi[b], B. Lestriez[b], D. Guyomard[b], L. Roué[a,*]

[a] INRS-Énergie, Matériaux et Télécommunications, 1650 boulevard Lionel-Boulet, Varennes, Québec, Canada J3X 1S2
[b] Institut des Matériaux Jean Rouxel, UMR 6502 CNRS – Université de Nantes, 2 rue de la Houssinière, BP 32229, 44322 Nantes Cedex 03, France

ARTICLE INFO

Article history:
Received 22 September 2011
Received in revised form
14 November 2011
Accepted 15 November 2011
Available online 23 November 2011

Keywords:
B-doped Si particles
Ball milling
Si-based negative electrode
Li-ion batteries
Resonant acoustic mixing

ABSTRACT

Boron-doped Si particles were prepared by high-energy ball-milling of pure B and Si in various proportions (0, 10^{20}, 10^{21}, 10^{22} and 10^{23} atoms B per mole Si). Despite the fact that only a fraction of the added B atoms were incorporated into the Si lattice, a significant decrease of the Si electrical resistivity was observed, leading to a minimum electrical resistivity of 0.13 Ω cm for the sample milled with 10^{21} atoms B per mole Si compared to 190 Ω cm for the boron-free sample. Electrochemical investigations focused on these two samples showed that the B-doping of Si does not improve significantly the performance of the composite Si-based electrode for Li-ion batteries in terms of cycle life, coulombic efficiency and high-rate chargeability. Through an analysis of anodic polarization curves, it was also shown that the delithiation reaction is mainly controlled by the Li-diffusion kinetics from a rate of ~4C on both electrodes. Lastly, it was shown that the use of a resonant acoustic mixer for the mixing of the (Si + carbon black + carboxymethyl cellulose) components increases the cycle life of the composite electrode.

1. Introduction

Li-ion batteries are presently the power source of choice for many portable electronic devices mainly due to their good storage capacities and long cycle life. They are now targeted for transportation and grid energy storage applications, which are more challenging in terms of battery storage capacity, lifetime, safety and cost than for the portable electronic market. In this context, silicon appears as a very attractive candidate to replace the carbon-based negative electrode in Li-ion batteries because of its ten times higher theoretical capacity (3572 mAh g^{-1}) and safer behaviour [1] than that of graphite electrodes. Unfortunately, its poor cycle life hinders its use in commercial Li-ion batteries. This is mainly due to the large volume change (up to ~300% [2]) occurring during the alloying/de-alloying reactions, which induces a loss of electrical contacts in the electrode. Numerous investigations have been undertaken to solve this problem [3,4] and in some cases, significant improvements in the cyclability of Si-based electrodes were obtained. For instance, we have recently achieved a cycle life as high as 800 cycles using commercial nanosized Si particles with carboxymethyl cellulose (CMC) binder in a half-cell with a capacity limitation of 1200 mAh g^{-1} of Si [5]. However, its practical use in full Li-ion cells is prevented due its low coulombic efficiency (~98%), which is attributed to the continuous formation of a solid electrolyte interface (SEI) upon cycling [6].

In addition, the insulating character of silicon may be a disadvantage by exacerbating the problem of electrical loss with cycling in the electrode and by inducing a large internal ohmic resistance, thus limiting its power capability. One way to enhance the electrical conductivity of Si particles is by coating them with conductive materials such as copper or carbon. However, this approach is not totally satisfactory due to the possible detachment of the coating from the Si surface caused by the severe volume change of the Si particles with cycling [7]. Another possible approach is the use of carrier-doped conductive Si materials but, to date, only a very few studies have examined this approach. For instance, Ohara et al. have shown that the use of n-type Si rather than pure Si for the preparation of vacuum-deposited Si thin films improves the high power capability and cycle life of the electrode [8]. Very recently, it was found that the electrode capacity is better retained, particularly at high C-rates, with doped rather than bare Si nanowires [9].

In the present study, boron-doped Si particles are prepared for the first time by high-energy ball-milling of pure B and Si powders in various proportions. This technique has the advantage of being a simple and low-cost method to produce doped-Si powder in large quantities. The selection of boron as doping element is firstly justified by its low reactivity in air facilitating its handling in contrast to phosphorus element for instance. In addition, our preliminary work with different types of dopants does not show significant difference between the use of a n-type dopant such as P or As and a n-type

* Corresponding author. Tel.: +1 514 228 6985; fax: +1 450 929 8102.
E-mail address: roue@emt.inrs.ca (L. Roué).

0378-7753/$ – see front matter © 2011 Elsevier B.V. All rights reserved.
doi:10.1016/j.jpowsour.2011.11.045

dopant such as B. The influence of the increase of the Si electrical conductivity with B-doping on the Si-based composite electrode performance for Li-ion batteries is presented.

2. Experimental

2.1. Material synthesis

Pure Si (99.999%, −20 mesh, Cerac) and B powders (95%, Laboratoire Mat) were used as starting materials. Samples were prepared with the following nominal boron concentrations (atom per mole Si): 0, 10^{20}, 10^{21}, 10^{22} and 10^{23} (equivalent to 0, 0.0167, 0.167, 1.64 and 14.3 at.% B, respectively). They are designated in the text by the terms B0, B20, B21, B22 and B23, respectively. The powder mixtures were loaded and sealed under argon atmosphere into a 55 ml stainless-steel vial containing two 11.1 mm and one 14.3 mm diameter stainless-steel balls. The ball-to-powder mass ratio was 5:1. Milling was performed for 20 h using a SPEX 8000 mixer. The milling yields (defined as the ratio of the powder masses after and before milling) were higher than 80% in all experiments, indicating moderate cold welding between the powder particles and the milling tools. No iron was detected by energy dispersive X-ray (EDX) analysis in the milled powders, reflecting the absence of significant erosion of the container and balls during milling.

2.2. Material characterization

X-ray diffraction (XRD) analyses were performed with a Bruker D8 diffractometer in a Bragg–Brentano geometry with Cu Kα radiation.

The specific surface area of the milled powders was measured using the Brunauer–Emmet–Tellet (BET) method with an adsorption analyser (Quantachrome) operating with krypton. Prior to the measurements, the samples were heated under vacuum at 200 °C for 2 h.

The morphology and composition of the milled powders were determined using a Jeol JSM-6300F scanning electron microscope (SEM) equipped with an energy dispersive X-ray (EDX) analyser.

The electrical resistivity of the milled powders was measured with a four-point-probe (Signatone). For these measurements, the milled powder (450 mg) was cold pressed at 20 tons cm^{-2} for 10 min and then sintered at 1000 °C under Ar atmosphere for 2 h in order to obtain dense pellet samples with a diameter of 11.3 mm and a thickness of ∼170 μm.

2.3. Electrochemical experiments

Milled Si-B powder was used as the active material, Super P carbon black (noted CB, 60 $m^2 g^{-1}$, TIMCAL) as the conductive agent, and carboxymethyl cellulose (CMC) (DS = 0.7, M_w = 90,000 Aldrich) as the binder. A mixture of 200 mg of active material + CB + CMC in a weight ratio of 80:12:8 was introduced into a silicon nitride vial containing three silicon nitride balls (9.5 mm diameter). Then, 0.5 mL of citric acid + KOH buffer solution at pH 3 was added and the mixture was milled at 500 rpm for 1 h using a Fritsch Pulverisette 7 mixer. The slurry was tape cast onto a 25 μm thick copper foil and dried for 12 h at room temperature and then 2 h at 100 °C in vacuum.

Two-electrode Swagelok cells were used for the cycling tests performed at 20 °C using an Arbin BT2000 cycler. The cells were assembled in a glove box under argon atmosphere and comprised (i) a 1 cm^2 disc of composite working electrode containing typically 0.7 mg of active material, (ii) a Whatman GF/D borosilicate glass-fiber sheet saturated with the electrolyte (1 M $LiPF_6$ dissolved in 1:1 dimethyl carbonate/ethylene carbonate (Novolyte)) and (iii) a 1 cm^2 Li metal disc as the negative and reference electrode. Cycling tests were performed in galvanostatic mode between 1 and 0.005 V versus Li^+/Li. Unless otherwise indicated, cycling was carried out at a current density of 600 mA g^{-1} of active material both in discharge (lithiation) and charge (delithiation).

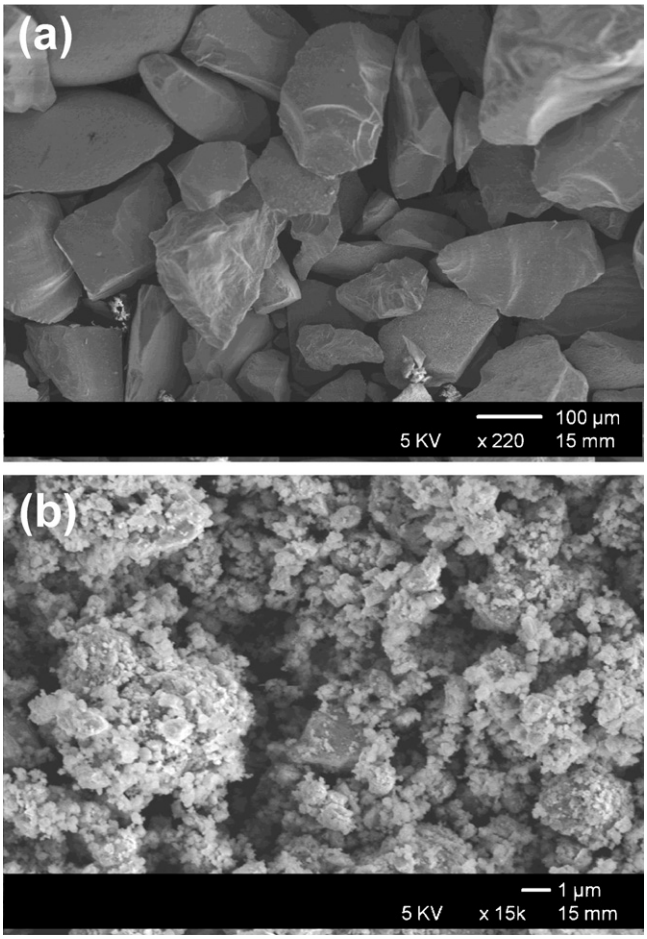

Fig. 1. SEM micrographs of the as-received Si powder (a) and B21 sample obtained after 20 h of milling (b).

The high-rate chargeability (HRC) of the electrode was determined according to the formula:

$$\mathrm{HRC}(\%) = \frac{C_x}{C_x + C_{0.6}} \times 100 \quad (1)$$

where C_x is the charge capacity obtained at a charge current density of xA g^{-1} (from 1 to 24 A g^{-1}) and $C_{0.6}$ is the residual charge capacity extracted at a charge current density of 0.6 A g^{-1} after the electrode was charged at xA g^{-1}. For these tests, the discharge capacity and discharge current density were fixed at 1200 mAh g^{-1} and 0.6 A g^{-1}, respectively. The stability of the charge capacity was confirmed on 10 cycles for each HRC measurement.

A three-electrode Swagelok cell (with the composite electrode as the working electrode and Li metal discs as the counter and reference electrodes) was used for the electrochemical impedance spectroscopy and linear sweep voltammetry experiments performed with a VMP3 multichannel workstation (BioLogic Science Instruments).

3. Results and discussion

3.1. Morphology

Fig. 1 shows SEM micrographs of the as-received Si powder (Fig. 1a) and B21 sample obtained after 20 h of milling (Fig. 1b). The

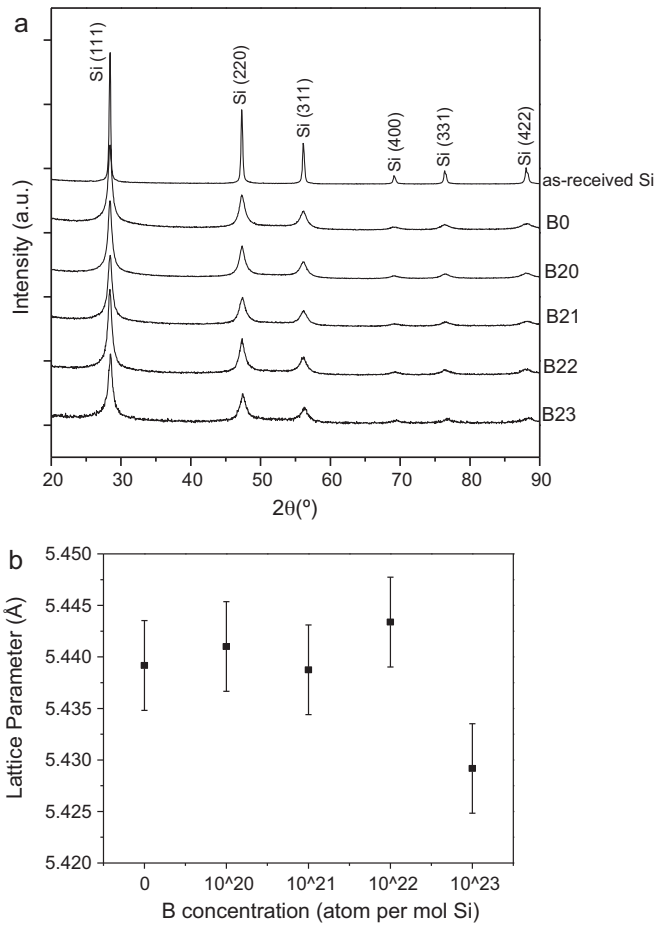

Fig. 2. (a) XRD patterns of the as-received Si and milled Si and Si-B samples. (b) Evolution of the lattice parameter of the Si phase as a function of the amount of added boron.

unmilled powder is made up of dense and large particles (>100 μm in size) whereas the milled powder consists of irregular and porous agglomerates made up of many small particles (<1 μm in size) more or less welded together, resulting from the repeated cold welding/fracturing processes occurring during ball milling. Similar morphology was observed for the different milled samples (not shown), indicating that boron addition does not affect the milling process. The BET surface area of the milled powders is $12 \pm 1\ m^2\ g^{-1}$, independent of their B content.

3.2. Crystal structure

The XRD patterns of the Si-B samples milled with different B contents are shown in Fig. 2a. The XRD pattern of the as-received pure Si power is also shown for comparison. All XRD patterns exhibit a series of peaks related to the face-centered-cubic (fcc) Si phase. No diffraction peaks corresponding to free boron are observed. However, this absence does not confirm the formation of B-doped Si because the boron phase was also not detected on the XRD patterns of the Si + B mixtures before milling (not shown) due its low amount and very low X-ray diffraction sensitivity. As expected, the diffraction peaks of the milled powders are broader than those of the as-received Si powder due to the decrease of the crystallite size and increase of the lattice strain through the milling process. The crystallite size (calculated using Sherrer's formula) is 11 ± 1 nm for all the milled powders compared to 35 nm for the unmilled Si. As shown in Fig. 2b, the lattice parameter of the fcc Si phase (calculated from the (1 1 1) peak position) does not vary significantly with B addition, except for the richer-B compound (B23) where a slight lattice decrease is observed, which indicates that some Si atoms are substituted by B atoms in the Si phase. The alloying process between Si and B is however incomplete because transmission electron microscopy (TEM) and electron energy-loss spectroscopy (EELS) investigations (not shown) indicated the presence of free boron (few nanometers in size) in the B23 sample. The formation of amorphous Si-B alloys may also occur. However, they were not detected from our TEM-EELS analyses.

Table 1
Measured and expected electrical resistivities of the Si-B samples.

Sample	B0	B20	B21	B22	B23
R measured (Ω cm)	190	0.18	0.13	0.20	0.30
R expected (Ω cm)	$>10^3$	$\sim10^{-2}$	$\sim10^{-3}$	$\sim10^{-4}$	$<10^{-4}$

3.3. Electrical resistivity

The electrical resistivity of the milled Si-B samples is presented in Table 1. From literature data [10], their expected electrical resistivity based on their nominal B content is also presented. The electrical resistivity of the boron-free sample (B0) is 190 Ω cm, which is much lower than expected for undoped Si ($>10^3$ Ω cm). This may be due to the formation through the milling process of numerous Si lattice defects associated with interstitial impurity atoms (O, Fe), vacancies, dislocations and/or grain boundaries. Ball milling with boron induces an additional and significant decrease of the Si electrical resistivity. The lowest electrical resistivity value (0.13 Ω cm) is observed with the B21 sample. However, the measured resistivity values of the Si-B samples are much higher than those expected from their nominal B content (by a factor 20–3000). This can be partially due to the contact resistances between the powder particles but above all, it reflects the fact that only a fraction of the added B atoms are incorporated in the Si lattice, as stated previously. This is supported by the increase of the electrical resistivity for the richer boron samples (B22 and B23) due to an expected higher amount of unalloyed insulating B atoms.

3.4. Electrochemical behaviour

The following electrochemical results are focused on the comparison between the boron-free sample (B0) and the B-doped sample having the lowest electrical resistivity (B21).

Fig. 3 shows the evolution with cycling of the specific charge (delithiation) capacity and coulombic efficiency (charge/discharge capacity ratio) of the B0 and B21 samples for a complete discharge (Fig. 3a and b) and for a discharge capacity limited at 1200 mAh g^{-1} of active material (Fig. 3c and d). No significant difference was observed between the two samples. They display a maximum charge capacity of 2300 ± 200 mAh g^{-1}, a mean capacity decay per cycle of 13 ± 2 mAh g^{-1}, a coulombic efficiency of 80% at the 1st cycle to 99% at the 150th cycle and a cycle life of 90 ± 5 cycles with a discharge capacity limited at 1200 mAh g^{-1}. This indicates that the insulating character of Si does not play a key role in the poor cycle life and low coulombic efficiency of Si-based electrodes.

Fig. 4a shows the evolution of the cumulated irreversible capacity with cycling for a discharge capacity limitation varying from 200 to 1200 mAh g^{-1}. This evolution is similar for the B0 and B21 electrodes. For both samples, the mean irreversible loss per cycle strongly depends on the discharge capacity, as highlighted in Fig. 4b. It increases abruptly when the discharge capacity limitation reaches 1200 mAh g^{-1}, leading to an irreversible loss rate of about 37 mAh g^{-1} per cycle compared to about 12, 6 and 3 mAh g^{-1} per cycle at discharge capacities of 800, 400 and 200 mAh g^{-1}, respectively. Note that the irreversible loss rate becomes much lower

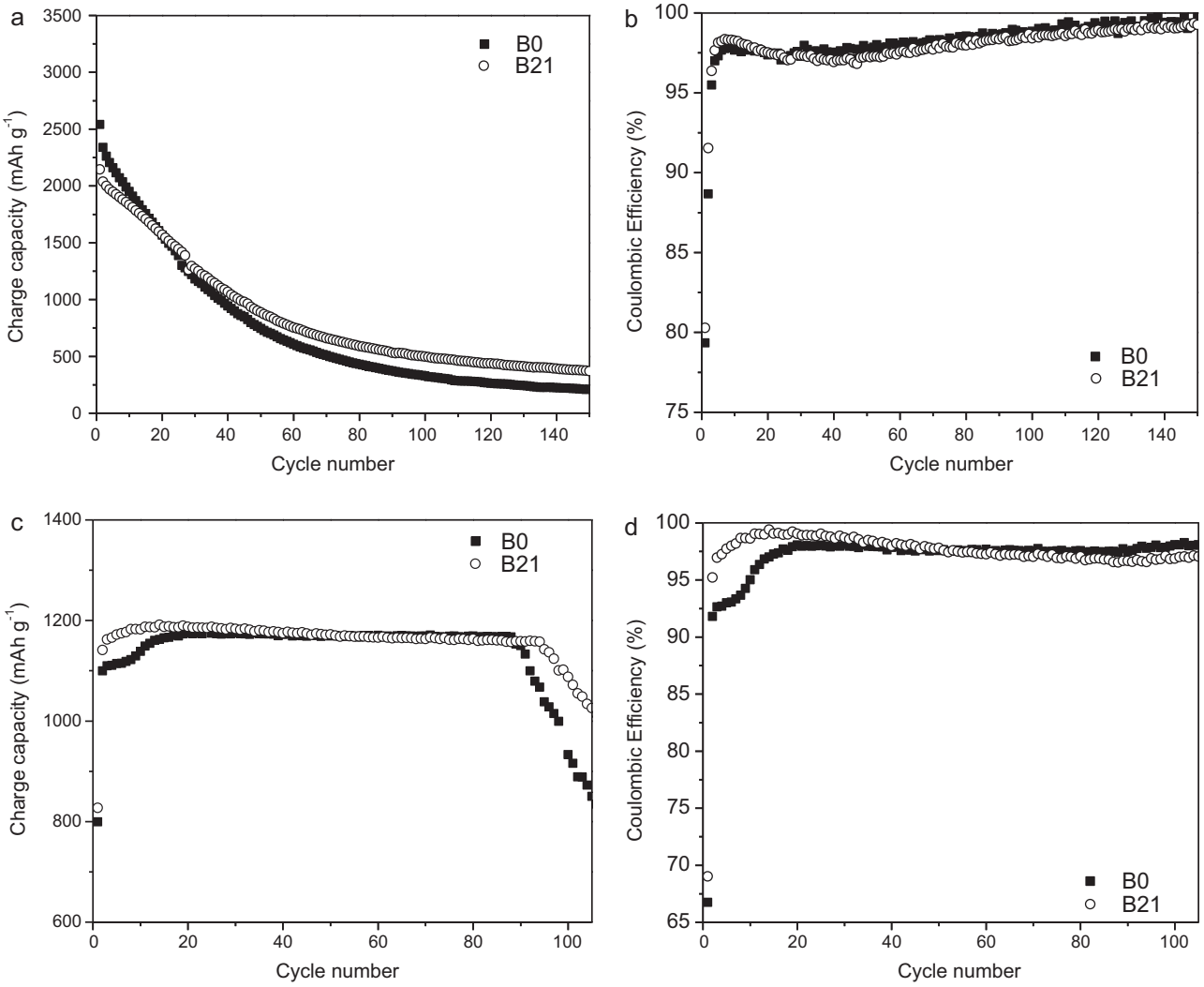

Fig. 3. Evolution with cycling of the charge capacity (a, c) and coulombic efficiency (b, d) of the B0 and B21 electrodes fully discharged (a, b) and discharged at 1200 mAh g^{-1} (c,d).

(from 4 to <1 mAh g^{-1} per cycle) for subsequent decreases of the capacity limitation. In comparison, electrodes prepared with nanometric Si using the same additive formulation displayed a linear increase of the irreversible loss rate with the increasing capacity limitation ranging from 400 to 1200 mAh g^{-1} and reached about 35 mAh g^{-1} per cycle at a discharge capacity of 1200 mAh g^{-1} [6]. It was demonstrated that the irreversible capacity was due to the loss of lithium trapped as lithium salt degradation products on the silicon particles and within the electrode pores rather than to the electronic disconnection of Li_xSi particles associated with their volume expansion. In the present case, the abrupt increase of the irreversible loss rate when the electrode capacity reaches 1200 mAh g^{-1} suggests that at this discharge capacity, the breaking point of the Si particles and/or the C-Si network related to the Si volume expansion may be reached, inducing the electrode decrepitation and thus the electronic disconnection of some Li_xSi particles. The B-doping of Si has no effect on this process in contrast to the use of nanometric Si particles.

Fig. 5 shows the high-rate chargeability of the B0 and B21 electrodes as a function of the charge current density. No significant difference was observed between the two electrodes. This means that the insulating character of Si has no effect on the electrode polarization resistance and thus, it is not a limiting factor in the power capability of our composite electrodes. A possible explanation is that lithiation of Si particles induces a significant enhancement of their electrical conductivity. This is supported by electrical conductivity measurements indicating that LiSi (prepared by high pressure synthesis) is a narrow-gap semiconductor (E_b = 0.057 eV) compared to Si (E_b = 1.11 eV) [11]. In situ conductivity measurements also showed that the conductivity of an amorphous Si electrode was increased by about 3.5 orders of magnitude during the course of lithium insertion [12]. However, our electrochemical impedance spectroscopy measurements show that the ohmic resistance (determined by the high-frequency intercept of the real axis in the Nyquist plot and considered to be primarily related to the electronic conductivity of the electrode components and ionic conductivity of the electrolyte) is similar for the B0 and B21 electrodes (R = 9–11 Ω) and does not vary significantly with the electrode discharge capacity (see Fig. 6). In other words, the variation of electronic resistivity of the Si particles does not have a significant influence on the ohmic resistance of the composite electrode, probably because of the presence of well-dispersed carbon black particles assuring an efficient electronic transport through the composite Si-based electrodes. In contrast, for Si electrodes prepared without carbon additive, their doping is likely to have a significant effect on their ohmic resistance and thus, on their electrochemical performance as shown with doped Si thin films [8] and doped Si nanowires [9].

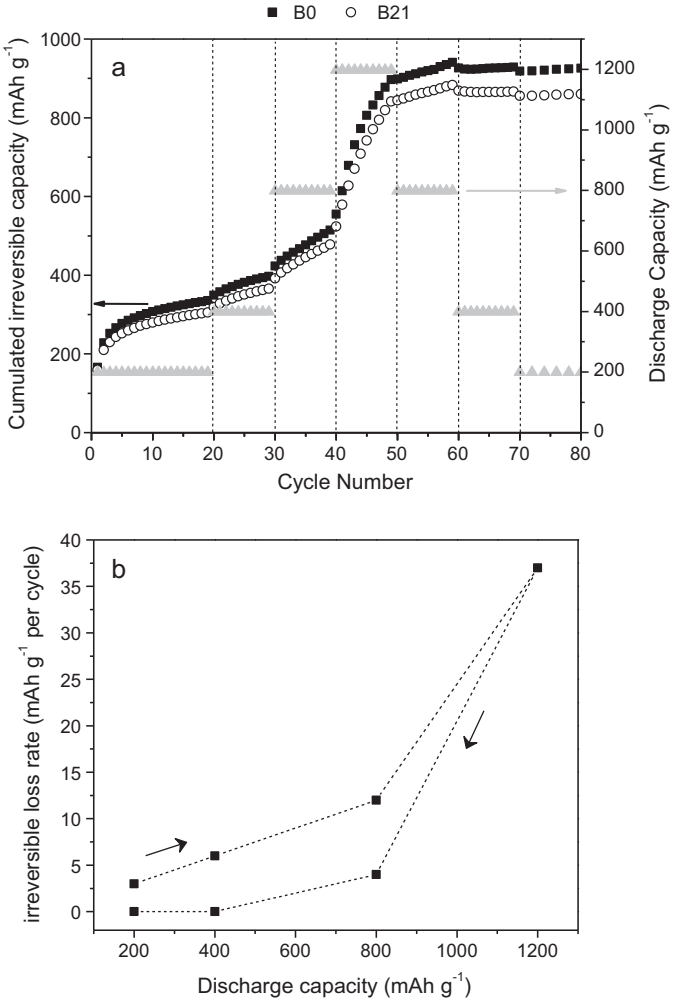

Fig. 4. (a) Evolution of the cumulated irreversible capacity as a function of the electrode discharge capacity for the B0 and B21 electrodes. (b) mean irreversible loss per cycle with respect to the electrode discharge capacity.

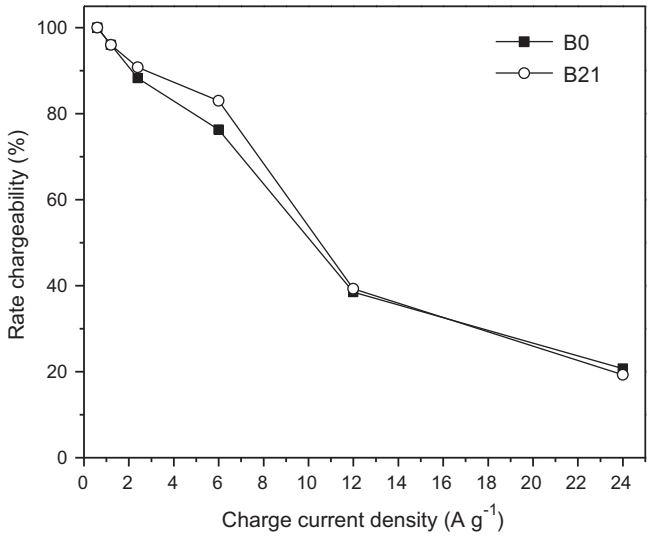

Fig. 5. High-rate chargeability with respect to the charge current for the B0 and B21 electrodes.

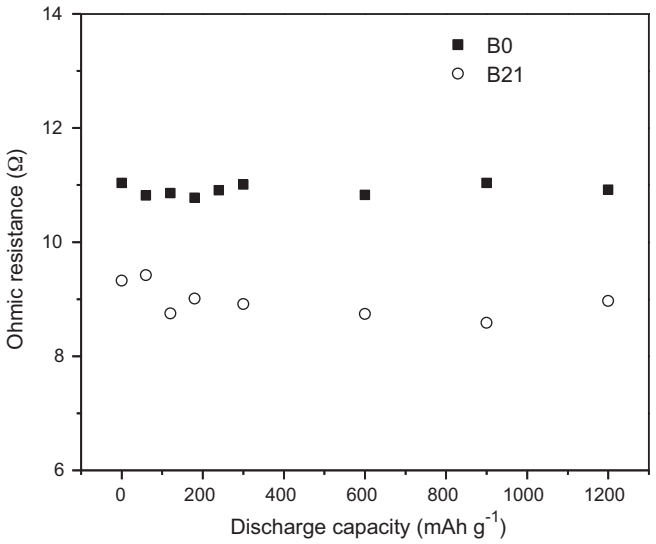

Fig. 6. Evolution of the ohmic resistance as a function of the discharge capacity for the B0 and B21 electrodes.

The two other resistance components likely to have a major influence on the electrode polarization resistance and thus on its high-rate chargeability are the charge-transfer resistance and the Li-diffusion resistance. In order to evaluate the influence of these two components on the electrode polarization resistance, anodic polarization experiments on the B0 and B21 electrodes were performed. Prior to the polarization measurements, the electrodes were cycled for 25 cycles at a limited discharge capacity of 1200 mAh g^{-1}, leading to a stabilized charge capacity. The electrodes were then discharged at 1200 mAh g^{-1} and remained in open circuit conditions for about 3 h up to stabilization of the open circuit potential. Anodic polarization curves were then obtained by scanning the electrode potential from 0 to 1000 mV (vs. open circuit potential) at 0.5 mV s^{-1}. The curves were corrected for the ohmic drop determined from impedance measurements, as indicated previously. Fig. 7a shows the resulting anodic polarization curves on B0 and B21 electrodes. The anodic current (i) is expressed per gram of Si. It increases as the overpotential (η) increases and reaches a limiting current (i_L) that results from mass transport limitation of the lithium atoms in the $SiLi_x$ alloy. The i_L values are listed in Table 2. The i_L value is not significantly different for the two electrodes (i_L around 4200 mA g^{-1}), confirming as expected that the B-doping of Si has no effect on the Li-diffusion kinetics.

The anodic overpotential η can be expressed as [13]:

$$\eta = \frac{RT}{(1-\alpha)} \ln\left(\frac{i}{i_0}\right) + \frac{RT}{(1-\alpha)} \ln\left(\frac{i_L}{i_L - i}\right) \quad (2)$$

where R is the gas constant, F is the Faraday constant, T is the temperature, α is the charge transfer coefficient and i_0 is the exchange current density. The first term on the right-hand side of Eq. (2) is the activation overpotential, η_a, due to the charge transfer resistance and the second term is the concentration overpotential, η_c,

Table 2
Limiting diffusion current (i_L), exchange current density (i_0) and charge transfer coefficient (α) values of the B0 and B21 electrodes.

Sample	i_L (mA g^{-1})	i_0 (mA g^{-1})	α
B0	4384	169	0.41
B21	4139	225	0.54

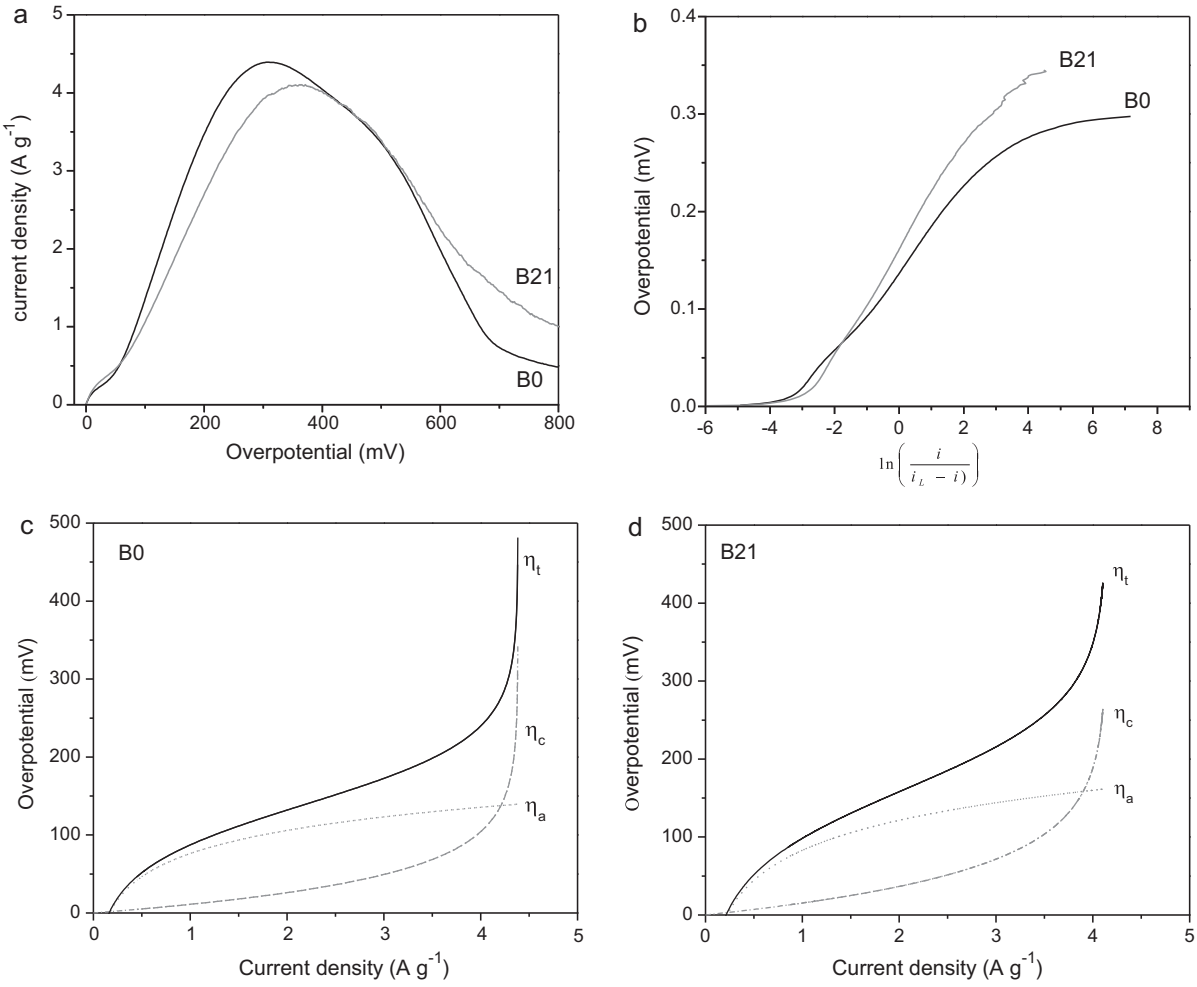

Fig. 7. (a) Anodic polarization curves for the B0 and B21 electrodes. Scan rate: 0.5 mV s^{-1}. (b) Overpotential as a function of ln $[i/(i_L - i)]$ for the B0 and B21 electrodes. (c) Evolution of the total overpotential (η_t), activation overpotential (η_a) and concentration overpotential (η_c) as a function of the charge current for the B0 electrode. (d) Evolution of the total overpotential (η_t), activation overpotential (η_a) and concentration overpotential (η_c) as a function of the charge current for the B21 electrode.

due to the Li-diffusion resistance. Rearranging Eq. (2) leads to the following expression [13]:

$$\eta = \frac{RT}{(1-\alpha)F} \ln\left(\frac{i_L}{i_0}\right) + \frac{RT}{(1-\alpha)F} \ln\left(\frac{i}{i_L - i}\right) \quad (3)$$

According to Eq. (3), a plot of η vs. ln $[i/(i_L - i)]$ produces a straight line in the middle range of overpotential as shown in Fig. 7b, permitting the determination of the α and i_0 values from the slope and intercept, respectively. These values are listed in Table 2. The exchange current density i_0 (which is inversely proportional to the charge transfer resistance R_{ct} according to the relation $i_0 = RT/FR_{ct}$) is slightly higher for the B21 electrode (i_0 = 225 mA g^{-1}) than for the B0 electrode (i_0 = 169 mA g^{-1}). This indicates that the B-doping of Si improves the charge-transfer kinetics but this improvement is quite limited. In addition, no significant difference is observed for the charge transfer coefficient ($\alpha \sim 0.4$–0.5).

In order to differentiate the contribution of the charge transfer resistance and Li-diffusion resistance to the anodic polarization, Eq. (2) was used to calculate the value of the activation overpotential (η_a) and the concentration overpotential (η_c). Their evolution as a function of the charge current is shown in Fig. 7c and 7d for the B0 and B21 electrodes, respectively. No significant difference is observed between the two electrodes, which is consistent with their similar high-rate chargeability performance shown in Fig. 5. As expected, η_a is higher than η_c at lower charge current densities while η_c becomes largely dominant at higher charge current densities for both electrodes. The delithiation reaction is assumed to be mainly controlled by the Li-diffusion process in the Li_xSi alloy when η_c exceeds η_a, *i.e.*, at a critical charge current density of about 4 A g^{-1}, which corresponds to a rate of ~4 lithium per hour (4C) on both electrodes. At lower charge current densities, the charge transfer reaction is assumed to be the rate-determining step. Note that for the discharge step and after prolonged cycling, kinetic limitations may differ due, for instance, to the formation of a blocking SEI layer on the Si particles, which inhibits the diffusion of the Li ions into the composite electrode pores as recently shown by Oumellal et al. [6].

3.5. *Influence of the mixing method for the preparation of the composite electrodes on their electrochemical performance*

The previous results have shown that the B-doping of Si has no significant influence on the composite electrode performance (*i.e.*, cycle life, coulombic efficiency and high-rate chargeability). In contrast, the mixing step of the different components (Si + CB + CMC) for the preparation of the composite electrode has a major impact on the electrode cycle life. This is illustrated in Fig. 8, which compares the evolution of the charge capacity with cycling at a limited discharge capacity of 1200 mAh g^{-1} for (i) an electrode prepared using the usual mixing protocol (*i.e.*, with a planetary mixer) as described in the Experimental section; (ii) an electrode prepared with a pre-mixing step of (Si + CB) for 5 min using an acoustic

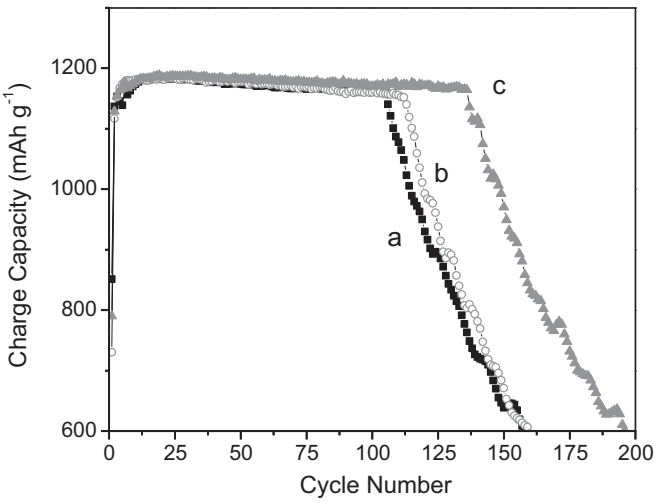

Fig. 8. Evolution with cycling of the charge capacity at a limited discharge capacity of 1200 mAh g^{-1} for a Si-based composite electrode (a) prepared without pre-mixing step; (b) prepared with a pre-mixing step of (Si + CB) for 5 min using an acoustic mixer and (c) prepared with a pre-mixing step of (Si + CB + CMC) for 5 min using an acoustic mixer.

mixer (LabRAM from Resodyn) followed by the usual mixing procedure and (iii) an electrode prepared with a pre-mixing step of (Si + CB + CMC) for 5 min using an acoustic mixer followed by the usual mixing procedure. Commercial micrometric Si powder (typically 1–20 μm in size) was used as active material in all cases. As shown in Fig. 8, the last electrode (curve *c*) displays the best performance with a cycle life of 135 cycles compared to about 105 cycles for the two first electrodes (curves *a* and *b*). On the other hand, the three electrodes present similar performance in terms of coulombic efficiency and high-rate chargeability (results not shown). These results tend to confirm the key role played by the CMC binder on electrode cycle life by favouring the networking process of the CB and Si particles during the composite electrode elaboration [5,14]. It is assumed that the pre-mixing of the (Si + CB + CMC) mixture using an acoustic mixer facilitates this networking process thanks to a better dispersion on the CMC component. The resonant acoustic mixing is a new approach to mixing and dispersion of materials [15]. It is distinct from conventional agitation found in a planetary mixer and from ultrasonic mixing in that the frequency of acoustic energy is orders of magnitude lower. The acoustic mixer operates at resonance and the resulting low frequency, high-intensity acoustic energy creates a uniform shear field throughout the entire mixing vessel and the mixing occurs on a microscale throughout the mixing volume. As a result, a rapid and very well dispersion of the mixture components occurs.

4. Conclusion

This work has shown that the increase of the electrical conductivity of Si particles by B-doping using high-energy ball milling has no significant effect on the electrochemical performance of composite (Si + CB + CMC) electrodes for Li-ion batteries. Actually, the presence of well-dispersed carbon black in moderate proportion (12 wt.%) seems to be sufficient for assuring an efficient electronic transport through the composite Si-based electrodes. On the other hand, the procedure for the composite electrode fabrication has a major effect on its electrochemical performance as illustrated by the improvement of the electrode cycle life thanks to a pre-mixing step of the (Si + CB + CMC) components using a resonant acoustic mixer. However, the performance of such electrode is still insufficient for a commercial use in Li-ion batteries. Further work in this direction (*i.e.*, in the optimization of the composite electrode manufacturing process) should lead to additional improvement in the performance of Si-based electrodes for Li-ion batteries.

Acknowledgements

The authors thank the Natural Sciences and Engineering Research Council (NSERC) of Canada, the Agence Nationale de la Recherche (ANR) of France, Bathium Canada, Metafoam Technologies and FPInnovations for supporting this work.

References

[1] Y. Wang, J. Dahn, Electrochem. Solid State Lett. 9 (2006) A340.
[2] L.Y. Beaulieu, T.D. Hatchard, A. Bonakdarpour, M.D. Fleischauer, J.R. Dahn, J. Electrochem. Soc. 150 (2003) A1457.
[3] U. Kasavajjula, C. Wang, A.J. Appleby, J. Power Sources 163 (2007) 1003.
[4] W.J. Zhang, J. Power Sources 196 (2011) 13.
[5] D. Mazouzi, B. Lestriez, L. Roué, D. Guyomard, Electrochem. Solid State Lett. 12 (2009) A215.
[6] Y. Oumellal, N. Delpuech, D. Mazouzi, N. Dupré, J. Gaubicher, P. Moreau, P. Soudan, B. Lestriez, D. Guyomard, J. Mater. Chem. 21 (2011) 6201.
[7] J.W. Kim, J.H. Ryu, K.T. Lee, S.M. Oh, J. Power Sources 147 (2005) 227.
[8] S. Ohara, J. Suzuki, K. Sekine, T. Takamura, J. Power Sources 136 (2004) 303.
[9] K. Kang, H.-S. Lee, D.-W. Han, G.-S. Kim, D. Lee, G. Lee, Y.-M. Kang, M.-H. Jo, Appl. Phys. Lett. 96 (2010) 053110.
[10] S.M. Sze, K.K. Ng, Physics of Semiconductor Devices, 3rd ed., John Wiley & Sons, 2006.
[11] L.A. Stearns, J. Gryko, J. Diefenbacher, G.K. Ramachandran, P.F. McMillan, J. Solid. State Chem. 173 (2003) 251.
[12] E. Pollak, G. Salitra, V. Baranchugov, D. Aurbach, J. Phys. Chem. C 111 (2007) 11437.
[13] A.J. Bard, L.R. Faulkner, Electrochemical Methods—Fundamentals and Applications, 2nd ed., John Wiley & Sons Inc., New York, 2001.
[14] B. Lestriez, S. Bahri, I. Sandu, L. Roué, D. Guyomard, Electrochem. Commun. 9 (2007) 2801.
[15] www.resodynmixers.com.